Eur. Phys. J. C 46, s01, 23–35 (2006)
Digital Object Identifier (DOI) 10.1140/epjcd/s2006-02-002-x

EPJ C direct
electronic only

Scientific Note

Reconstruction of the signal amplitude of the CMS electromagnetic calorimeter

The CMS Electromagnetic Calorimeter Group

P. Adzic[3], R. Alemany-Fernandez[13], C.B. Almeida[13,14], N.M. Almeida[13], G. Anagnostou[2], M.G. Anfreville[11], I. Anicin[3], Z. Antunovic[30], E. Auffray[10], S. Baccaro[28,29], S. Baffioni[25], D. Barney[10], L.M. Barone[29], P. Barrillon[15], A. Bartoloni[29], S. Beauceron[11], F. Beaudette[10], K.W. Bell[8], R. Benetta[10], M.J. Bercher[25], U. Berthon[25], B. Betev[38], R. Beuselinck[15], A. Bhardwaj[7], C. Biino[33], S. Bimbot[25], J. Blaha[35], P. Bloch[10], S. Blyth[6], P. Bordalo[13], A. Bornheim[26], J.M. Bourotte[25,10], D. Britton[15], R.M. Brown[8], R. Brunelière[10], P. Busson[25], T. Camporesi[10], N. Cartiglia[33], F. Cavallari[29], M. Cerutti[25], D. Chamont[25], P. Chang[6], Y.H. Chang[6], C. Charlot[25], S. Chatterji[7], E.A. Chen[6], R. Chipaux[11], B.C. Choudhary[7], D.J. Cockerill[8], C. Collard[25], C. Combaret[35], F. Cossutti[34], S. Costantini[29], J.C. Da Silva[13], I. Dafinei[29], G. Daskalakis[15], G. Davatz[38], A. Debraine[25], D. Decotigny[25], A. De Min[17], K. Deiters[36], M. Dejardin[11], R. Della Negra[35], G. Della Ricca[34], P. Depasse[35], J. Descamp[11], G. Dewhirst[15], S. Dhawan[23], M. Diemoz[29], G. Dissertori[38], M. Dittmar[38], L. Djambazov[38], L. Dobrzynski[25], S. Drndarevic[3], M. Dupanloup[35], M. Dzelalija[30], J. Ehlers[38], H. El Mamouni[35], A. Elliott-Peisert[10], I. Evangelou[12], B. Fabbro[11], J.L. Faure[11], J. Fay[35], F. Ferri[17], P.S. Flower[8], G. Franzoni[17,18], W. Funk[10], A. Gaillac[25], C. Gargiulo[29], S. Gascon Shotkin[35], Y. Geerebaert[25], F.X. Gentit[11], A. Ghezzi[17], J. Gilly[25], A.S. Giolo-Nicollerat[38,10], A. Givernaud[11], S. Gninenko[20], A. Go[6], N. Godinovic[31], N. Golubev[20], I. Golutvin[9], R. Gomez-Reino[10], P. Govoni[17], J. Grahl[18], P. Gras[11], J. Greenhalgh[8], J.P. Guillaud[1], M. Haguenauer[25], G. Hamel-de-Montechenault[11], M. Hansen[10], H.F. Heath[5], J.A. Hill[8], P.R. Hobson[16], D. Holmes[5], A.G. Holzner[38], G.W. Hou[32], B. Ille[35], Q. Ingram[36], A. Jain[13], P. Jarry[11], C. Jauffret[25], M. Jha[7], M.A. Karar[25], S.K. Kataria[22], V. Katchanov[27], B.W. Kennedy[8], K. Kloukinas[10], P. Kokkas[12], M. Korjik[19], N. Krasnikov[20], D. Krpic[3], A. Kyriakis[2], M. Lebeau[10], P. Lecomte[38], P. Lecoq[10], M.C. Lemaire[11], M. Lethuillier[35], W. Lin[6], A.L. Lintern[8], A. Lister[38], V. Litvin[26], E. Locci[11], A.B. Lodge[8], E. Longo[29], D. Loukas[2], D. Luckey[38], W. Lustermann[38], C. Lynch[5], C.K. Mackay[5], M. Malberti[17], D. Maletic[3], I. Mandjavidze[11], N. Manthos[12], A. Markou[2], H. Mathez[35], A. Mathieu[25], V. Matveev[20], G. Maurelli[35], E. Menichetti[33], P. Meridiani[29], P. Milenovic[3], G. Milleret[25], P. Mine[25], M. Mur[11], Y. Musienko[4,19], A. Nardulli[38], J. Nash[15,10], H. Neal[23], P. Nedelec[1], P. Negri[17], F. Nessi-Tedaldi[38], H.B. Newman[26], A. Nikitenko[15], M.M. Obertino[33,18], R.A. Ofierzynski[10,38], G.C. Organtini[29], P. Paganini[25], M. Paganoni[17], I. Papadopoulos[12], R. Paramatti[10,29], N. Pastrone[33], F. Pauss[38], P. Poilleux[25], I. Puljak[31], A. Pullia[17], J. Puzovic[3], S. Ragazzi[17], S. Ramos[13], S. Rahatlou[29], J. Rander[11], K. Ranjan[7], O. Ravat[35], M. Raymond[15], P.A. Razis[24], N. Redaelli[17], D. Renker[36], S. Reucroft[4], J.M. Reymond[11], M. Reynaud[35], S. Reynaud[10], T. Romanteau[25], F. Rondeaux[11], A. Rosowsky[11], C. Rovelli[17], R. Rusack[18], S.V. Rusakov[21], M.J. Ryan[15], H. Rykaczewski[38], T. Sakhelashvili[36,39], R. Salerno[17], M. Santos[13,14], C. Seez[15], I. Semeniouk[25], O. Sharif[16], P. Sharp[15], C. Shepherd-Themistocleous[8], S. Shevchenko[26], R.K. Shivpuri[7], G. Sidiropoulos[12], D. Sillou[1], A. Singovski[18], Y. Sirois[25], A.M. Sirunyan[37], B. Smith[8], V.J. Smith[5], M. Sproston[8], H. Suter[38], J. Swain[4], T. Tabarelli De Fatis[17], M. Takahashi[15], R.J. Tapper[5], A. Tcheremoukhine[9], I. Teixeira[13,14], J.P. Teixeira[13,14], O. Teller[10], C. Timlin[15], F.A. Triantis[12], S. Troshin[27], N. Tyurin[27], K. Ueno[32], A. Uzunian[27], J. Varela[13,10], N. Vaz Cardoso[13], P. Verrecchia[11], P. Vichoudis[10], S. Vigano[17], G. Viertel[38], T. Virdee[15,10], M. Wang[32], A. Weinstein[26], J.H. Williams[8], I. Yaselli[16], A. Zabi[15], N. Zamiatin[9], S. Zelepoukine[27,38], M. Zeller[23], L.Y. Zhang[26], Y. Zhang[15], K. Zhu[26], R.Y. Zhu[26]

[1] Laboratoire d'Annecy-le-Vieux de Physique des Particules, 74941 Annecy-le-Vieux, France
[2] Institute of Nuclear Physics "Demokritos", 153 10 Attiki, Greece
[3] "Vinca" Institute of Nuclear Sciences and Faculty of Physics of University of Belgrade, 11000 Belgrade, Serbia and Montenegro
[4] Northeastern University, Boston MA 02115-5096, USA
[5] Bristol University, Bristol BS8 1TL, UK
[6] National Central University, Chung-Li, Taiwan, ROC
[7] Delhi University, Delhi 110 007, India
[8] CCLRC, Rutherford Appleton Laboratory, Didcot OX11 0QX, UK
[9] Joint Institute for Nuclear Research, 141980 Dubna (Moscow Region), Russia
[10] European Organization for Nuclear Research, CERN, 1211 Geneva 23, Switzerland

[11] CEA/Saclay, 91191 Gif-sur-Yvette cedex, France
[12] University of Ioannina, 451 10 Ioannina, Greece
[13] Laboratório de Instrumentação e Física Experimental de Partículas, 1000-149 Lisboa, Portugal
[14] Instituto de Engenharia de Sistemas e Computadores, 1000-029 Lisboa, Portugal
[15] Imperial College, London SW7 2BZ, UK
[16] Brunel University, Middlesex UB8 3PH, UK
[17] Università degli Studi Milano-Bicocca and INFN-Sezione di Milano, 20126 Milano, Italy
[18] University of Minnesota, Minneapolis MN 55455, USA
[19] Research Institute for Nuclear Problems, Byelorussian State University, 220050 Minsk, Byelorussia
[20] Institute for Nuclear Research, Russian Academy of Sciences, 117312 Moscow, Russia
[21] Lebedev Physical Institute, Russian Academy of Sciences, 117924 Moscow, Russia
[22] Bhabha Atomic Research Centre, Mumbai 400 085, India
[23] Yale University, New Haven CT 06520-8121, USA
[24] Cyprus University, 1678 Nicosia, Cyprus
[25] Laboratoire Leprince-Ringuet, Ecole Polytechnique, 91128 Palaiseau Cedex, France
[26] California Institute of Technology, Charles C. Lauritsen Laboratory, Pasadena CA91125, USA
[27] State Research Center, 142284 Protvino (Moscow Region), Russia
[28] ENEA–CR Casaccia, 00060 S. Maria di Galeria, Roma, Italy
[29] Università "La Sapienza", Dipartimento di Fisica and INFN-Sezione di Roma, 00185 Roma, Italy
[30] Split University, PMF, 21000 Split, Croatia
[31] Technical University of Split, FESB, 21000 Split, Croatia
[32] National Taiwan University, 106 Taipei, Taiwan ROC
[33] Università di Torino, Dipartimento di Fisica and INFN-Sezione di Torino, 10125 Torino, Italy
[34] Università di Trieste, Dipartimento di Fisica and INFN-Sezione di Trieste, 34127 Trieste, Italy
[35] Institut de Physique Nucléaire, IN2P3-CNRS and Université C. Bernard Lyon I, 69622 Villeurbanne, France
[36] Paul Scherrer Institut, 5232 Villigen, Switzerland
[37] Yerevan Physics Institute, 375036 Yerevan 36, Armenia
[38] Institute for Particle Physics, ETH Zürich, 8093 Zürich, Switzerland
[39] On leave from High Energy Physics Institute, Tblisi, Georgia

Received: 10 April 2006 / Revised version: 13 April 2006 /
Published online: 16 June 2006 – © Springer-Verlag / Società Italiana di Fisica 2006

Abstract. The amplitude of the signal collected from the $PbWO_4$ crystals of the CMS electromagnetic calorimeter is reconstructed by a digital filtering technique. The amplitude reconstruction has been studied with test beam data recorded from a fully equipped barrel supermodule. Issues specific to data taken in the test beam are investigated, and the implementation of the method for CMS data taking is discussed.

1 Introduction

The compact muon solenoid (CMS) [1] is a general purpose detector to be installed at the 14 TeV proton–proton collider, LHC, under construction at CERN and due to start operation in 2007. The electromagnetic calorimeter (ECAL) [2] of the detector is a hermetic homogeneous calorimeter made of 61 200 scintillating lead tungstate ($PbWO_4$) crystals mounted in the central barrel part, closed by 7324 crystals in each of the two end-caps. The barrel part of the ECAL consists of 36 supermodules, each covering half the barrel length and 20° in azimuth and containing 1700 crystals together with the associated electronics channels. The use of high density $PbWO_4$ crystals [3] has allowed the design of a calorimeter which is fast, has fine granularity and is radiation resistant – all important characteristics in the LHC environment. Avalanche photodiodes (APDs) are used as photodetectors in the barrel and vacuum phototriodes in the end-caps [4, 5].

The electrical signal from the photodetectors is amplified and shaped by a multi-gain preamplifier (MGPA) before digitization by ADCs at a frequency of 40 MHz [6]. For each channel three signals, resulting from amplification with three different gains, are simultaneously digitized in three ADCs. Further logic chooses the highest non-saturated digital value, allowing a dynamic range of about 5×10^4 from the least significant bit of about 35 MeV to saturation at 1.7 TeV in the barrel.

The data read out consists of a series of consecutive digitizations, corresponding to a sequence of samplings of the signal at 40 MHz. It is envisaged that a time frame of 10 consecutive samplings will be read out in LHC operation, and the signal amplitude must be reconstructed using these samplings.

The complete process of signal amplification followed by signal digitization and amplitude reconstruction should not degrade the energy resolution of the calorimeter other than by the inevitable introduction of noise. The simplest method of reconstructing the amplitude is to take a sampling on the signal pulse maximum as the measurement. Reading out a larger number of samples allows identification of out of time (other bunch crossing) pile-up and an event-by-event subtraction of the pedestal. It also allows more sophisticated digital processing of the signal to improve the signal to noise ratio, and a measurement of the signal timing. We report here on the performance of a method which implements a digital filter.

Test beam data taken in the H4 beam line at the CERN SPS in October and November 2004 using electron beams with a range of momenta between 20 and 250 GeV$/c$, have been used to investigate the method of amplitude reconstruction. A supermodule was installed on a movable table which allowed the beam to be directed at any part of it. Electrons were incident at an angle $\simeq 3°$ to the direction of the crystal axis in both transverse directions, reproducing the average incident angle of particles emerging from the collision region in LHC running. Plastic scintillator counters were used to trigger the read-out. The position of the incident electrons in the transverse directions was determined by four planes of scintillating fiber hodoscopes. An earlier test of a complete supermodule installed in the same beam area is described in [7].

The test beam provides data for the verification of the amplitude reconstruction method, but these data differ in an important way from those which will be taken in running at the LHC. In the test beam the scintillation signals have a random timing with respect to the ADC clock, while during LHC operation the ADC clock will be synchronous with the bunch crossing. It is necessary to identify and investigate effects which are specific to asynchronous running before being able to achieve full performance with test beam data. The coefficients, or weights, of the digital filter used to reconstruct the signal amplitude are optimized to minimize the noise contribution, but reconstruction of the amplitude from the time frames read out in asynchronous running imposes additional requirements. If these are not met, an error proportional to the signal amplitude is introduced which becomes a constant term in the energy resolution function (σ_{E}/E).

In order to determine the phase between the signal peak and the sampling time, a TDC was used to measure the delay between the trigger and the 40 MHz ADC digitization clock. Verification of the performance of the amplitude reconstruction method envisaged in synchronous data taking at the LHC has been made by selecting test beam events within a narrow window around a chosen phase.

In this note, the principle of the digital filter method is described first. The derivation of the weights is described, as well as an investigation of the impact of pile-up events. The algorithm intended for use in CMS data taking is discussed, and then issues specific to asynchronous operation in the test beam are identified and discussed. Fuller details of the mathematical formalism used to determine the weights of the digital filter can be found in an appendix.

2 The weights method

The method used to reconstruct the amplitude from the digitized samples is based on a digital filtering technique. An estimate of the signal amplitude, $\hat{\mathcal{A}}$, is computed from a linear combination of discrete time samples:

$$\hat{\mathcal{A}} = \sum_{i=1}^{N} w_i \times S_i \,, \tag{1}$$

where w_i are the weights, S_i the time sample values in ADC counts, and N is the number of samples used in the filtering, with the index i running over the time samples. The weights w_i are obtained by minimizing the variance of $\hat{\mathcal{A}}$ (see Appendix A). Requiring that the estimator of the amplitude, $\hat{\mathcal{A}}$, be not just proportional, but equal to the amplitude, A, implies that

$$\sum_{i=1}^{N} w_i f_i = 1 \,, \tag{2}$$

where f_i is the value of the function, $f(t)$, describing the time development of the signal pulse in time, t, at the time t_i of sample i. The function is normalized to have an amplitude of 1.

The question of how precisely the function $f(t)$ needs to be matched to the shape and timing of each channel to enable the derivation of a set of weights giving satisfactory amplitude reconstruction is one that we attempt to answer in this paper.

A form of the function $f(t)$ that provides a good description of the electronics signal is a digital representation (profile histogram) directly built from the test beam data. An example of such a representation, obtained using an electron beam of 120 GeV, is shown in Fig. 1. The rise time is about 50 ns, which corresponds to the 10 ns decay time of the crystal scintillation folded with and the 40 ns shaping time of the MGPA. In the test beam the data were read out so that at least three samples, which we refer to as presamples, were taken before the start of the signal.

The weights are extracted by minimization of the χ^2, which is given by

$$\chi^2 = \sum_{i,j} (S_i - G_i) \times \mathbf{C}^{-1}_{ij} \times (S_j - G_j) \,, \tag{3}$$

where

- S_i is the sample magnitude in ADC counts recorded at the time t_i;

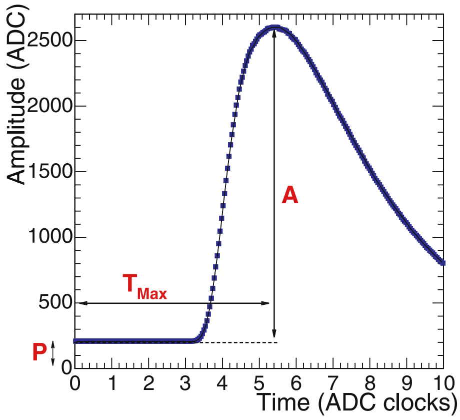

Fig. 1. Profile of the signal pulse from a crystal of the supermodule using an electron beam of 120 GeV. The peaking time T_{Max}, the pedestal P and the amplitude of the signal A are shown

- The signal pulse is described by G_i which is a function that depends on different parameters: $G_i = G_i(A, P, T_{\mathrm{Max}})$ where A is the true amplitude, P is the pedestal and T_{Max} is the peaking time (see Fig. 1);
- $\mathbf{C}$ is the covariance matrix representing the noise correlation between time samples i and j, obtained from data where no signal is present.

If there is no noise correlation between time samples ($\mathbf{C} = \mathbb{1}\sigma^2$, where σ is the single sample noise defined below) and the pedestal and peaking time are known (so that $G = G(A) = Af(t)$), the optimal weights are given by the formula

$$w_i = f_i / \sum_{j=1}^{N} f_j^2 \,. \qquad (4)$$

The derivation of this formula is given in Appendix A.

These weights give the best estimation of the amplitude A. Since the samples contain information about the peaking time and the pedestal also, two further sets of weights can be derived to measure these parameters.

3 Optimization

3.1 The samples considered

The reconstruction of the signal amplitude could use a single sample taken at the signal peak. In synchronous running the pulse maximum time, represented by the parameter T_{Max}, can be adjusted so that the peak coincides with one of the samplings. If the pedestal is determined independently and subtracted from the maximum, this one sample gives the pulse amplitude. This technique has the advantage of being relatively insensitive to any possible jitter on T_{Max} (this will be discussed in Sect. 4). However, using a larger number of samples allows some reduction of the noise contribution.

When considering the weights obtained assuming no noise correlations between time samples, as given by (4), the square root of the variance, $\sigma_{\hat{\mathcal{A}}}$, of the estimated amplitude is

$$\sigma_{\hat{\mathcal{A}}} = \sigma / \sqrt{\sum f_i^2} \,, \qquad (5)$$

where σ is the noise present on a single digitization, the single sampling noise. Thus, an increase of the number of samples will reduce the value of the noise in the reconstructed amplitude. Furthermore, better noise reduction is achieved if samples near the peak, containing more signal, are used. The noise on the reconstructed amplitude should be reduced from that of a single sampling by a factor $\sqrt{\sum w_i^2}$. Calculating weights from the functional representation shown in Fig. 1, assuming no noise correlation between samples, it is found that the use of five samples should give a noise reduction $\simeq 0.6$ (see Fig. 2) with little improvement when more samples are used. The 1 sample option takes the sampling on the peak, for the 2 sample option the sampling before the peak is added, for the 3 sample option the next sampling after the peak is added, and for 4 sample and higher options the remaining samplings after the peak are added in consecutive order. The figure also shows the expected noise reduction if the noise correlation seen in the test beam is assumed, and the weights are calculated using the measured covariance matrix (see Sect. 3.2.2).

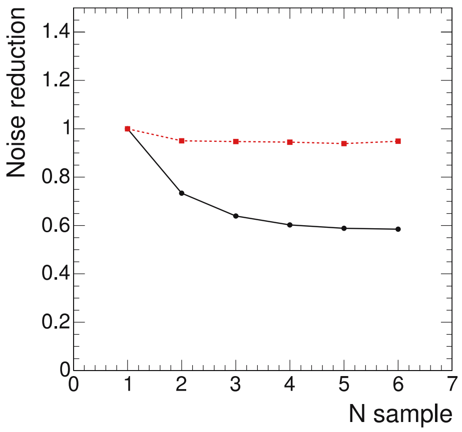

Fig. 2. Expected noise reduction ($\sqrt{\sum w_i^2}$) as a function of the number of samples used for the reconstruction in the case of no noise correlations between time samples (*solid line*) and in the case of the correlations found in test beam data (*dashed line*)

3.2 Noise reduction

The noise reduction expected from using many samples in a situation where there is no noise correlation between samplings is not fully realized when the amplitude reconstruction algorithm is applied to real data. This occurs because of the presence of noise which is correlated between samples. This is partly due to pickup noise which is also, to some degree, correlated between channels; it has a much lower frequency than the 40 MHz sampling frequency and appears as a small event-to-event fluctuation in the level of the signal baseline or pedestal. The digital filter can be configured to subtract the pedestal using the information present in the presamples. Such a digital filter effectively removes the baseline fluctuation [8]. The noise performance of different implementations were compared using test beam data.

3.2.1 Measurement of the noise

The method was implemented in two different forms.

- The “5 weights” implementation:
  The 5 weights method uses five samples as defined in the previous section to reconstruct the signal amplitude. The pedestal is determined independently and its value is subtracted from the samples before reconstruction.
- The “pedestal-subtracting weights” implementation:
  The pedestal-subtracting weights method uses $3+5$ weights applied to three samples before the signal pulse

(the three presamples) and five samples during the pulse. The weights are calculated by minimizing (3) with $G = G(A, P) = Af(t) + P$. It may be noted that in this situation $\sum w_i = 0$. Such a set of weights performs a subtraction of the pedestal on an event-by-event basis.

For completeness, a $3+1$ weights pedestal-subtracting implementation has been studied. The single weight is applied to the sample on the peak. This allows the demonstration of the impact of dynamic baseline subtraction in its simplest form.

The noise is the root mean square deviation of the reconstructed amplitude when no signal is input. Thus the ECAL noise is measured by examining the variation of the reconstructed amplitude when random triggers, data taken with no signal (often called "pedestal runs"), are reconstructed. Table 1 shows the noise measured when using these implementations of the method for a single channel, and for sums of channels corresponding to matrices of 3×3 and 5×5 crystals (typical of ECAL shower reconstruction). Also shown, for comparison, is the single sampling noise (as defined in Sect. 3.1). Results for sums of channels are given because energy is reconstructed in the ECAL from such sums: the noise in the sums represents the noise seen when shower energy is measured. Noise coherent between channels will increase the total measured in such sums above the quadratic sum of the contributions measured in component channels. A total of 1200 events from six different runs were used and the mean values of noise in eight different locations across the supermodule are given. When using the 5 weights method, the pedestal values for all the crystals were directly measured from the data by taking the average value, over a run, of the first presample.

The results given in Table 1 show that the lowest noise is achieved by the pedestal-subtracting weights. This implies the presence of the low frequency noise, mentioned above, which is removed by the dynamic pedestal subtraction.

Comparing the noise seen in a single channel with that seen in sums of 3×3 and 5×5 channels, the magnitude of the noise correlation between channels in a matrix of crystals can be appreciated. With the pedestal-subtracting weights filter the total noise seen in a sum of 9 (25) channels is almost exactly 3 (5) times the noise seen in a single channel, showing that the coherent noise between channels has been effectively removed. This noise is not suppressed when the average pedestal values for each channel are subtracted for each event. The total noise in a sum of 25 channels is reduced by 20% as compared to what is measured by reconstruction followed by pedestal subtraction using an average pedestal. Dynamic subtraction of the pedestal also avoids the effects from variation of the pedestal over time.

The table also allows comparison between the use of $3+5$ and $3+1$ pedestal-subtracting weights. Using five samples in the signal, rather than one, results in a slightly lower noise value.

Using pedestal-subtracting weights the average value of the noise measured in 1000 channels of the supermodule is roughly 40 MeV/channel (1 ADC count $\cong$ 37 MeV). Nevertheless it can be seen from the table that this implementation of the weights method is not able to reduce the noise contribution by the factor of 0.6 expected when there is no noise correlation. Clearly there is noise correlation, so the covariance matrix might be used to derive a more optimized set of weights. An investigation of the use of the covariance matrix is described in the next subsection.

3.2.2 Use of the covariance matrix

The covariance matrix represents the correlation of the noise between time samples. It is defined by

$$\mathbf{C}_{ij} = \langle n_i \times n_j \rangle \,, \tag{6}$$

where $n_i = S_i - P_i$ is the difference between the sample value and its mean (the pedestal) for sample i in the absence of a signal. The notation $\langle\rangle$ indicates an average over many events. Thus the diagonal elements $C_{ii} = \sigma^2$ are the squared single sampling noise. This matrix can be built using a pedestal run and then used in the determination of an optimized set of weights (3).

The same six pedestal runs previously used for the results in Table 1 were processed to extract the matrix coefficients. An adequate number of events was used to limit the statistical error on these coefficients. Strong correlations are present between samples which are close in time, as should be expected since the sampling period is shorter than the electronics shaping time. The MGPA preamplifier noise in the highest gain range is dominated by parallel noise from a feedback resistor and so the correlation between pairs of samples monotonically reduces as the time

Table 1. Noise in ADC counts measured in a single channel and in arrays of 3×3 and 5×5 channels for various weight implementions described in the text. The statistical errors on the measurements are also given

Method	Noise (ADC counts)		
	1×1	3×3	5×5
single sampling	1.20±0.01	3.7±0.04	6.5±0.1
5 weights	1.11±0.02	3.8±0.1	6.7±0.1
3+1 pedestal subtracting weights	1.13±0.03	3.4±0.1	5.7±0.1
3+5 pedestal subtracting weights	1.07±0.02	3.2±0.1	5.4±0.1

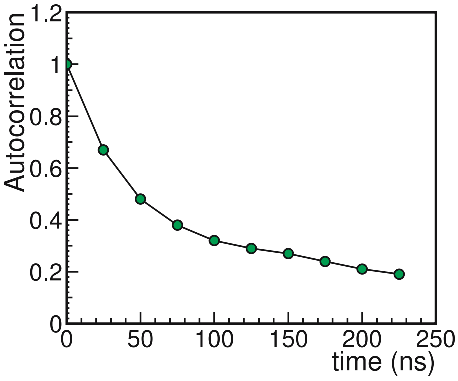

Fig. 3. Measurements of the autocorrelation function at intervals of 25 ns, obtained from the top row of the normalized covariance matrix, averaged for six channels. The *lines* joining the points are intended to guide the eye

interval between them increases, until it reaches a residual value which corresponds to the low frequency pickup noise. The decrease of the correlation follows an exponential law whose time constant is related to the shaping time of the electronics. The correlations and the form of the covariance matrix can be displayed by plotting the values in the top row of the normalized covariance matrix, $(\mathbf{C}_{1,j}/\sigma^2)$ (see Fig. 3). These values are measurements of the autocorrelation function at time intervals corresponding to multiples of the sampling time.

The optimization of the weights using the noise covariance matrix results in giving more weight to the sample on the peak. The samples near the peak have less weight, and the weights applied to samples further away become almost insignificant. The expected noise reduction from the single sampling noise is 0.94 (see Fig. 2) and not 0.6 as calculated for the case of no noise correlation. Pedestal-subtracting weights can also be derived using the covariance matrix.

Table 2 gives the noise measured when the covariance matrix is used to derive the weights. The results shown are the mean values of the noise measured in 8 different locations across the supermodule. Comparing the results in the table with those shown in Table 1 it can be seen that the use of the covariance matrix allows a small decrease in the noise contribution, but the improvement over pedestal-subtracting weights without its use is marginal and all further results in this paper have been obtain without its use.

4 Amplitude reconstruction for CMS running

An investigation of the amplitude reconstruction method required for use with CMS data taken during LHC running, where the sampling is synchronous with the signals, is described in this section.

4.1 Signal shape and timing

It has been observed in test beam data that the signal shapes and timing differ from crystal to crystal. The main difference lies in the parameter T_{Max} which shows an rms dispersion of roughly 3 ns across the supermodule. This dispersion is due to the imperfect precision with which the relative timing of the channels was adjusted at the start of the 2004 beam test. Using a representation of the signal with a T_{Max} different from that of the actual signal to determine the weights changes the reconstructed amplitude. Defining $\Delta T_{\mathrm{Max}} = T_{\mathrm{Max}}^{\mathrm{rep}} - T_{\mathrm{Max}}$, where $T_{\mathrm{Max}}^{\mathrm{rep}}$ is the time of maximum of the signal representation used to derive the weights, a timing difference of $\Delta T_{\mathrm{Max}} = 1$ ns causes approximately 0.1% bias on the reconstructed amplitude when using the $3+5$ weights method (see Fig. 4). The $3+1$ weights method is less sensitive to the timing because we have chosen to adjust the timing so that a sample is taken on the peak. The signal samplings of the $3+5$ weights are then mostly after the peak. The small bias caused by a timing difference, if constant with time, will be absorbed into the intercalibration of the ECAL channels. However, systematic drift or variation of the time of the signal pulse maximum would result in a variation of the channel response with time. To avoid such a variation the parameter T_{Max} needs, in the future, to be carefully controlled and monitored. T_{Max} can be precisely measured during data taking (see Sect. 4.2) and adjusted for each front end card (25 channels) with a 1 ns precision, by changing a parameter downloaded to the card.

Figure 5 (left) shows the energy resolution as a function of the difference in timing between the signal representation used to determine the weights and the signal. The signal amplitude has been reconstructed using the $3+5$ pedestal-subtracting weights. To simulate synchronous running, test beam data have been analyzed taking only events in a single 1 ns bin of phase, where the sampling phase is such that the signal maximum coincides with the second signal sampling. Since the same set of events is used

Table 2. Noise in ADC counts measured in a single channel and arrays of 3×3 and 5×5 channels for two subtracting-weights implementations of the amplitude reconstruction method where the covariance matrix has been used to derive the weights. The statistical errors on the measurements are also given

Method	Noise (ADC counts)		
	1×1	3×3	5×5
5 weights	1.05 ± 0.02	3.3 ± 0.1	5.9 ± 0.1
3+5 pedestal subtracting weights	1.05 ± 0.02	3.0 ± 0.1	5.2 ± 0.1

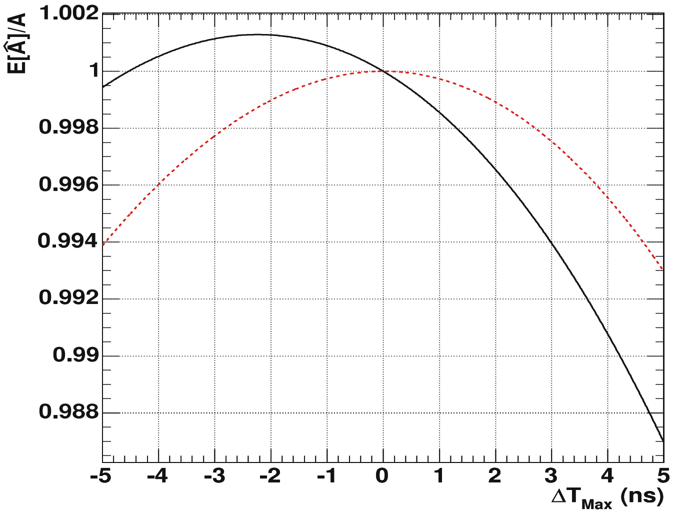

Fig. 4. Reconstructed amplitude over true amplitude, $E[\hat{A}]/A$, as a function of timing difference ΔT_{Max}. The *solid line* shows the value obtained with $3+5$ pedestal-subtracting weights, and the *dashed line* shows the value obtained using $3+1$ pedestal-subtracting weights

in each case, the uncertainties on the individual results are correlated. A range of ±3 ns was used for the scan, corresponding to the rms dispersion of T_{Max} observed in the supermodule. The resolution is on average better for $\Delta T_{\mathrm{Max}} < 0$. However, this is a result of the large 0.65 ns jitter on the phase measurement. When $\Delta T_{\mathrm{Max}} > 0$ there is more sensitivity to timing as has been seen in Fig. 4. There is no strong dependence on ΔT_{Max}, as there is in the case of aynchronous reconstruction (shown later in Fig. 13).

To study the sensitivity to differences between the pulse shape of the representation used to derive the weights and that of the signal, a homothetic transformation characterized by a contraction factor, C, has been applied to the time scale $(t \to t + C \times (t - T_{\mathrm{Max}}))$ of the representation used to derive the weights. Fits to the data indicate that the channel to channel pulse shape variation within the supermodule tested corresponds to an rms dispersion of 0.05 for the parameter C. Figure 5 (right) shows that the resolution is unaffected by variations of C within a range corresponding to a much larger dispersion in pulse shapes than observed in the supermodule. Other variations of the pulse shape have been tried (varying independently the rise and fall times) and yield the same conclusion.

These results suggest that, in the case of synchronous running, the same reference signal representation can be used to derive a single set of weights to be used for the signal amplitude reconstruction of all channels.

4.2 Time measurement

As already mentioned, the phase between pulse maximum and digitization clock can be adjusted for each front end card (25 channels) to 1 ns precision. In the supermodule tested in 2004 it was observed that the additional dispersion of the channels within each front end card was less than 1 ns. The measurement of the time of maximum used for adjusting the front end cards and then for monitoring the stability of the setting can be made using weights. The set of weights which is derived to do this is different from the set of weights used to determine the amplitude (see Appendix A). They measure the time difference between the nominal time of maximum and the actual time of maximum. As in Sect. 2, weights are obtained by minimizing χ^2. Because of the linear expansion used, the time of maximum is obtained without bias only if the difference between the nominal time of maximum and the actual time of maximum is small. The bias on the estimated time due to the linear expansion is shown in Fig. 6 as a function of the time difference, δt, between the nominal time of maximum and the actual time of maximum. The bias is less than 20 ps if $|\delta t| < 1$ ns.

The variance of the time measurement, $V(\delta t)$, can be parameterized by

$$V(\delta t) \simeq \frac{a^2}{c^2 + (A/\sigma)^2} + b^2\,, \tag{7}$$

where a, b, c are three parameters and σ is the single sampling noise. The parameter $c = \sqrt{V(A)/\sigma^2} \simeq 0.94$ becomes negligible when $A \gg \sigma$. Parameter a is related to $\sqrt{V(A\delta t)/\sigma^2}$ and strongly depends on the position of the

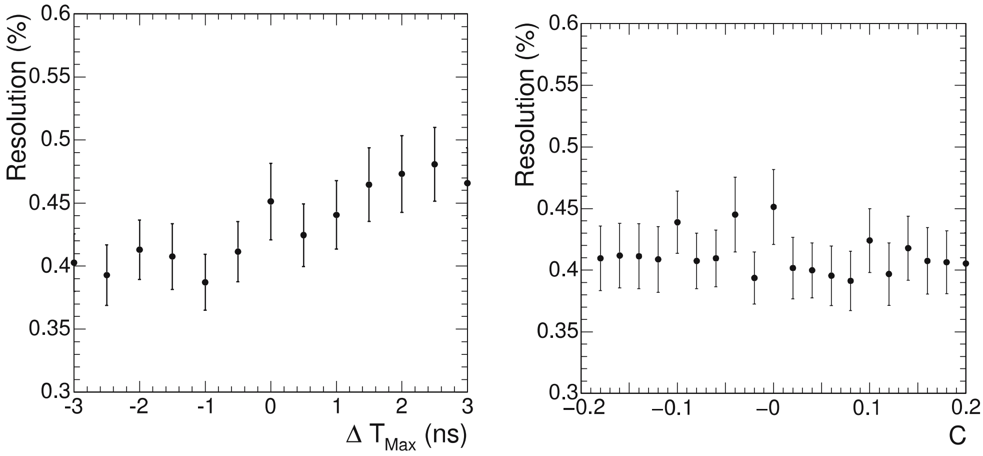

Fig. 5. (*Left*) Energy resolution in a 3×3 matrix of crystals measured with a 120 GeV electron beam, as a function of ΔT_{Max}. (*Right*) Energy resolution as a function of the contraction factor, C

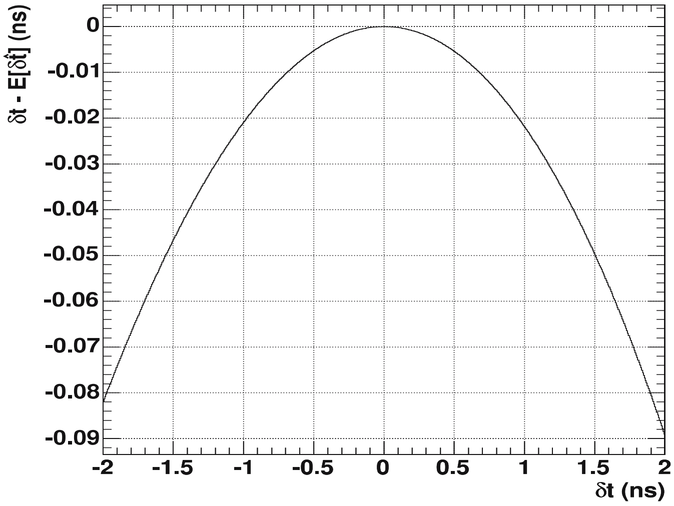

Fig. 6. Time bias, $\delta t - E[\delta t]$, introduced by the linear approximation, as a function of δt

nominal time of maximum with respect to the sampling time, i.e. the phase choice, because $V(A\delta t)$ is proportional to the sum of the derivatives of the signal as a function of time. The parameter b appears when the functional representation does not exactly reproduce the true signal, and limits the precision of measurement for large signals.

During the 2004 test beam data taking it was not possible to directly measure the timing resolution as a function of the signal amplitude because of an additional jitter introduced by measurement of the trigger time. However, the achievable time resolution can be extracted by looking at the resolution of the measured time difference between two channels. Figure 7 shows the resolution on the time difference between two channels as a function of the quadratic sum of the time resolutions for the individual channels. Assuming that the parameters a, b and c are the same for both channels the variance on the time difference between the channels, $V(t_1 - t_2)$, is

$$V(t_1 - t_2) \simeq V(\delta t_1) + V(\delta t_2) \simeq a \times \left(\frac{\sigma_1^2}{A_1^2} + \frac{\sigma_2^2}{A_2^2} \right) + 2 \times b\,. \tag{8}$$

The value of the constant term $b = 0.11$ ns is obtained by fitting this function to the data points in Fig. 7.

In summary, it can be concluded that taking reconstructed pulses with $A > 50 \times \sigma$, i.e. energy > 2 GeV, T_{Max} can be measured to a precision much better than 1 ns, allowing monitoring of the peak position to the required precision (see Sect. 4.1). The time resolution is dominated by the constant term for pulses with $A > \frac{a}{b}\sigma \simeq 500 \times \sigma$. In the 2004 beam test the constant term was measured to be 0.11 ns.

4.3 Effect of pile-up events

Shaped signals cover several bunch crossings. When using the multi-weights method described above, up to 8 time samples are used. Pile-up noise will occur if additional particles reaching the calorimeter cause signals which overlap these samples, and if sufficiently large may affect the set of optimum weights, as has been found for other calorimeters [9].

The magnitude of pile-up noise expected at low luminosity ($\mathcal{L} = 2 \times 10^{33}\,\mathrm{cm}^{-2}\,\mathrm{s}^{-1}$) was simulated and studied using CMS reconstruction software. The single sampling electronics noise was set to 40 MeV per channel. Correlations between time samples were simulated to reproduce the correlations observed in the supermodule tested in the beam. Pile-up noise was simulated using minimum bias events generated between -5 and $+3$ bunch crossings before and after signal. The average number of minimum bias events used per bunch crossing was 3.5. Figure 8 shows the reconstructed amplitude observed with and without pile-up in the absence of any signal (the signals from the pile-up

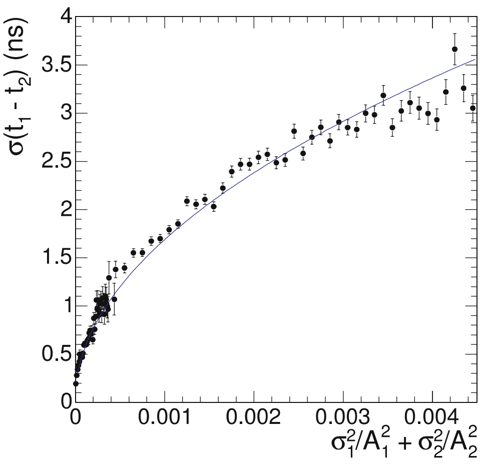

Fig. 7. Resolution on time difference between two crystals as a function of the sum of inverse square amplitudes. The fit is made assuming that the parameters a and b of (7) are the same for both crystals

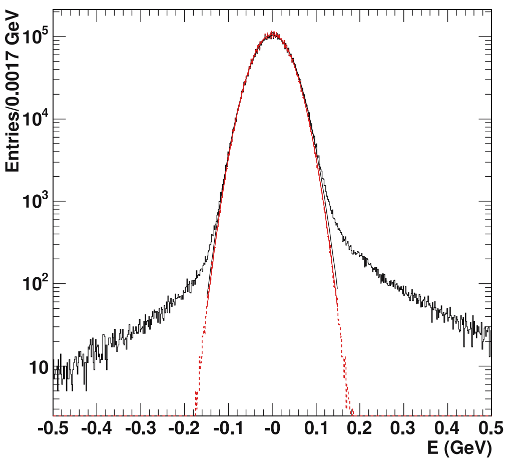

Fig. 8. Reconstructed amplitude in ECAL barrel channels in the absence of a signal, without pile-up (*dashed histogram*) and with pile-up (*solid histogram*). A Gaussian of width 40 MeV is superimposed on the *dashed histogram*

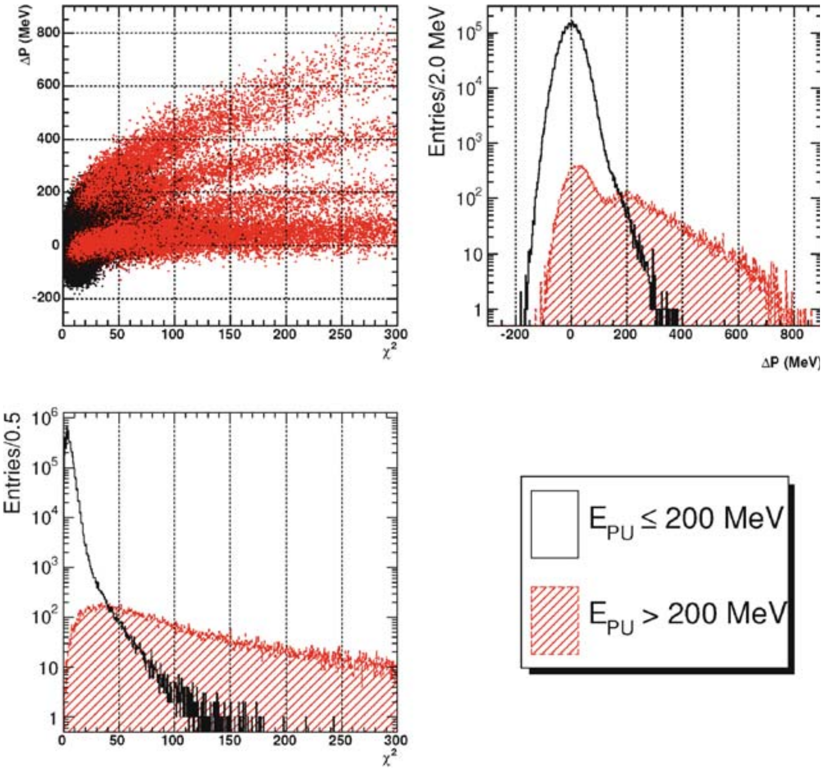

Fig. 9. Distribution of ΔP versus χ^2 in the ECAL barrel, together with the projections of these variables plotted as histograms. The distributions are shown separately for pulses which include out of time pile-up particles with an energy greater than 200 MeV and those which do not. The bands in the scatter plot correspond to particles from different bunch crossings

are considered as noise). The figure shows that at low luminosity the pile-up noise is small with respect to electronics noise.

High energy pile-up particles from bunch crossings different from that of the signal can be identified using cuts on χ^2_{Min} (defined in Appendix A) as well as the variable ΔP which corresponds to the difference between the reconstructed baseline and the expected one (evaluated from pedestal runs). Distributions of reconstructed signal pulses with and without high energy (> 200 MeV) pile-up particles are shown in Fig. 9 as a function of χ^2_{Min} and ΔP. The bands shown in the scatter plot for events containing high energy pile-up correspond to particles from different bunch crossings. By applying cuts on the variables χ^2_{Min} and ΔP it is possible to remove out of time pile-up signals that deposit a significant amount of energy.

4.4 Amplitude reconstruction at high energy

At high energy, the data read-out contains samples recorded with different gains. The pedestal value of the ADC digitizing the lower gain signal is not the same as the pedestal value of the ADC digitizing the higher gain signal. The three presamplings thus do not give a measure of the pedestal of the ADC used for the most significant samplings of the signal (i.e. close to the peak). Thus a pedestal-subtracting weights method cannot be used. There is also little to be gained from using many weights, since noise is negligible at these energies (the gain range change takes place at about 150 GeV for barrel channels). It is sufficient to measure the signal amplitude with a single sampling. In synchronous running the sample recorded on the peak is pedestal subtracted and then multiplied by the gain ratio (the relative calibration with respect to the highest gain range). The gain ratios must be determined precisely to avoid a degradation of the resolution and the introduction of non-linearity.

5 Application to asynchronous test beam data

In the test beam the ADC clock and the signal are asynchronous, and the implementation of the amplitude reconstruction needs to be elaborated to deal with this. The phase between the trigger (and thus the signal pulse) and the 40 MHz ADC clock was measured with a TDC. The data are sorted into 25 bins of 1 ns according to the measured phase. A different set of weights is determined and used for each of the bins. This imposes an additional severe requirement: the same amplitude must be reconstructed in all phase bins.

5.1 Effect of channel to channel differences in signal timing and shape

The effect of differences in signal timing and shape between the signal pulse and the signal representation is dependent on the phase bin and can be studied by comparing the results obtained using weights derived from an average representation of the signal pulse with those obtained using weights derived from a profile built using the data collected

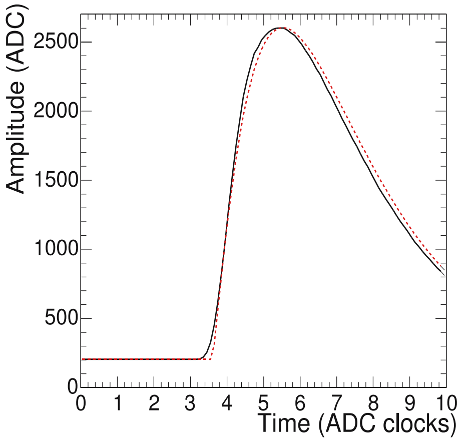

Fig. 10. Signal pulses for a 120 GeV electron beam: the *solid line* shows the profile of the signal in the channel under study, and the *dotted line* shows the average representation of the signal

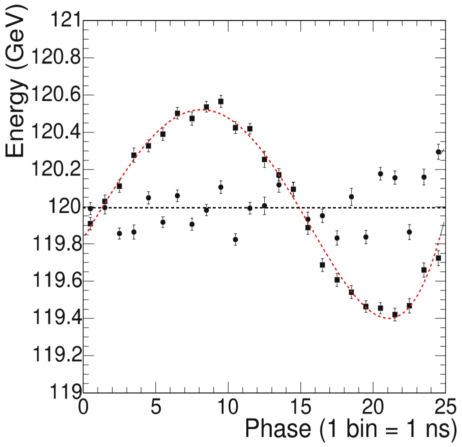

Fig. 11. Average reconstructed amplitude summed in a 3×3 matrix of crystals as a function of the phase using weights obtained with the average representation of the signal (*squares*) and the signal profile from the channel under study (*circles*). The polynomial fit and straight line are shown to guide the eye

from the investigated channel. The average representation is obtained by fitting the data from a large number of channels with an analytic formula and then taking the average of the fitted parameter values. A comparison between the average representation and a particular profile is shown in Fig. 10. The shapes are different in the rising edge, and the time of maximum also differs. Two collections of 25 sets of weights (one set for each phase bin) are extracted, one for each representation, and used to reconstruct the amplitude.

Figure 11 shows the average reconstructed amplitude summed in a 3×3 matrix of crystals in each of the 25 1 ns phase bins. The average reconstructed amplitude, obtained from a Gaussian fit to the peak of the reconstructed amplitude distribution, is plotted as a function of the phase for both sets of weights. Using the weights derived from the average representation results in a bias in the

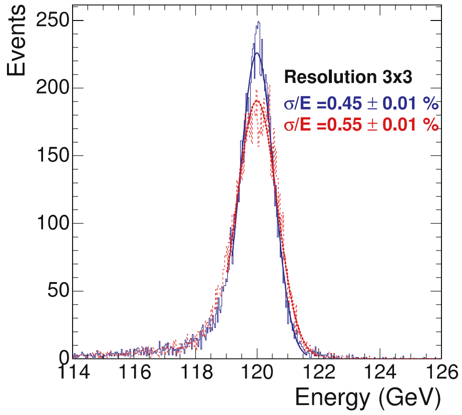

Fig. 12. Distribution of the reconstructed amplitude in a 3×3 matrix for a 120 GeV beam using the weights derived from an average representation of the signal pulse (*dashed histogram*) and the true profile of the signal in the crystal studied (*solid histogram*). Truncated Gaussian fits are superimposed on both distributions and are used to derive the energy resolution: 0.55% for the dashed histogram, and 0.45% for the solid histogram. (Asynchronous data using all phase bins)

reconstructed amplitude which varies with phase and ultimately degrades the energy resolution as can be seen in Fig. 12. When the weights are derived using the signal description specific to each channel, the resolution is as good as the one obtained in a single 1 ns bin. The bias visible in Fig. 11, when the weights used are those derived from the average representation, could also be corrected using the fitted line, leading to a comparable resolution.

5.1.1 Relative importance of shape and timing

The relative importance of differences in signal timing and shape between the signal pulse and the signal representation used to derive the weights has been studied. As in Sect. 4.1 the signal in each channel is characterized by its peaking time T_{Max} and its width. Figure 13 shows the energy resolution measured when the weights used to reconstruct the amplitude are derived from signal representations with peaking times and widths which differ from those of the actual signal. The situation here differs from that shown in Fig. 5, since here data in all 25 phase bins are being reconstructed, using 25 sets of weights. This is a reconstruction of the full asynchronous test beam data set, whereas Fig. 5 refers to a reconstruction of data in a single phase bin, simulating synchronous data.

When the weights are derived using a signal representation that has a width contraction factor 0.05 (the rms dispersion in a supermodule) different from the signal width the resolution is degraded from 0.45% to 0.52%. When the weights are derived using a signal representation that has a T_{Max} 3 ns (the rms dispersion in the supermodule) different from that of the signal, the resolution is degraded from 0.45% to 0.70%. Thus the most significant cause of the

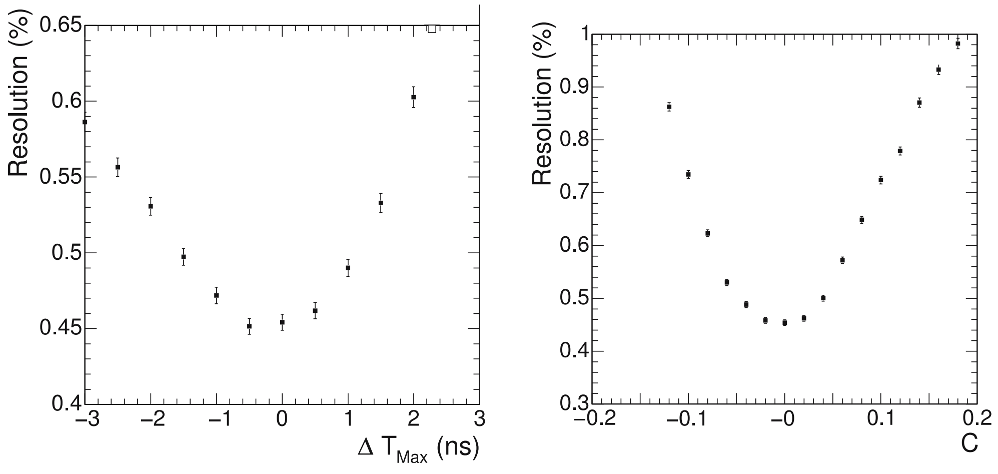

Fig. 13. Energy resolution in a 3×3 matrix of crystals for a 120 GeV electron beam (*left*), as a function of ΔT_{Max}, and (*right*) as a function of the contraction factor, C

resolution degradation resulting from the use of an average signal pulse representation to derive the weights for reconstruction of asynchronous data is a mismatch of signal timing. It should be possible, in the future test beam data taking, to adjust the signal timing to within 1 ns. Alternatively, the mistimings could be categorized, and a number of different sets of weights used.

5.2 Timing jitter

As described in Sect. 5, different sets of weights are used for events in different bins of phase. The TDC measurement is used to decide which set of weights should be used. However, an rms uncertainty of approximately 0.65 ns on the TDC phase measurement was observed. This results in an additional smearing of amplitudes which degrades the energy resolution.

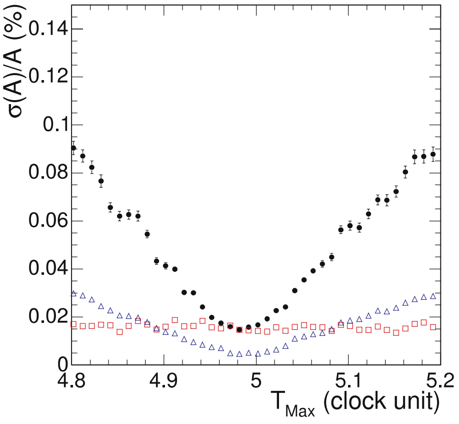

Fig. 14. Amplitude measurement spread due to jitter as a function of pulse maximum time. *Solid circles* and *open squares* correspond to simulated events with a timing jitter of 0.65 ns. The *solid circles* are obtained when the standard amplitude reconstruction is used, whereas the *open squares* result from the use of jitter-compensating weights. The *open triangles* correspond to standard amplitude reconstruction when the jitter is equal to 0.2 ns, as expected in CMS

The derivation of the weights can be modified to account for small event-to-event variations of the pulse timing relative to the clock, or jitter, and produce what we call “jitter-compensating” weights (see Appendix A). Figure 14 shows the results of a study using simulated signal pulses to determine the effect of jitter on the constant term as a function of pulse maximum time for both the standard amplitude reconstruction method and jitter-compensating weights. The effect of jitter in the case of CMS running ($\simeq 0.2$ ns due to the bunch length) is also shown. The results demonstrate that the effect of jitter will be negligible in CMS running, without the use of jitter-compensating weights, especially if the sampling is performed on the peak.

Figure 15 shows the distribution of reconstructed amplitude summed in a 3×3 matrix of crystals using pedestal-subtracting weights and pedestal-subtracting weights with jitter compensation. The improvement observed when using jitter-compensating weights has motivated the choice of using these special sets of weights to extract performance results from test beam data taken in 2004.

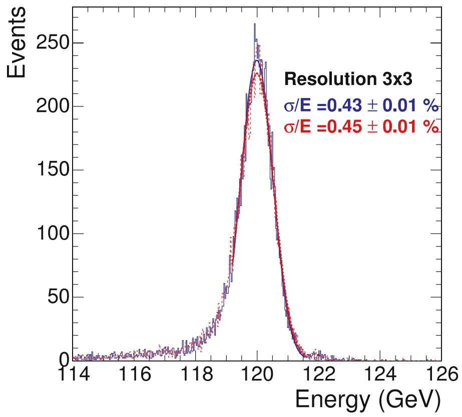

Fig. 15. Distribution of the reconstructed amplitude, for asynchronous data using all phase bins, summed in a 3×3 matrix of crystals using pedestal-subtracting weights with (*solid histogram*, $\sigma/E = 0.43\%$) and without (*dashed histogram*, $\sigma/E = 0.45\%$) jitter compensation

6 Conclusion

Reconstruction of the signal amplitude in the CMS ECAL can be performed using digital filtering techniques. Using an implementation with dynamic pedestal subtraction, the measured noise in a single channel is 40 MeV, and coherent noise between channels is effectively removed so that the noise measured in a 3×3 (5×5) matrix of crystals is about 120 MeV (200 MeV). Additional noise induced by pile-up events was investigated with simulated data and shown to be negligible at low luminosity.

Studies of the test beam data collected in 2004 with a fully equipped supermodule allowed investigation of the importance of the shape and timing of the reference signal representation used to derive the weights, as well as the effect of timing jitter on the resolution. The impact on the resolution of the shape and timing of the reference signal representation used to derive the weights has been clearly demonstrated to be caused by the asynchronous data taking mode in the test beam. The necessity to reconstruct the same amplitude for all values of the phase imposes severe constraints on the tolerable variation of timing and pulse shape between channels. The poor time resolution of the phase measurement used in the 2004 test beam data taking also requires use of more complex and sophisticated techniques to avoid degradation of the resolution.

In synchronous running, as will be the case at LHC, a single set of weights can be used to reconstruct the amplitude in all the ECAL channels and timing information can be provided using an additional set of weights. The time measurement can be used to monitor possible shifts of the signal timing.

Appendix : Weights derivation

In order to derive optimal weights, a least squares method is used. The χ^2, defined in Sect. 2, can be written in matrix notation as

$$\chi^2 = (\mathbf{S} - \mathbf{G}(A, \delta t, P))^{\mathrm{T}} \mathbf{C}^{-1} (\mathbf{S} - \mathbf{G}(A, \delta t, P)) , \qquad \text{(A.1)}$$

where $\mathbf{S}$ is a vector of the time samples S_i with N elements, $\mathbf{C}$ is the noise covariance matrix, and $\mathbf{G}(A, \delta t, P)$ is a vector describing the mean of the measurements, modeled by

$$G(t_i; A, \delta t, P) = A f(t_i + \delta t) + P . \qquad \text{(A.2)}$$

Here A is the amplitude of the signal, $f(t)$ is the function which corresponds to the time development of the signal pulse, δt is a possible timing jitter, and P is the pedestal. If δt is small enough, (A.2) can be linearized:

$$G(t_i; A, \delta t, P) \simeq A f(t_i) + (A\delta t) \frac{\mathrm{d}f}{\mathrm{d}t}(t_i) + P , \qquad \text{(A.3)}$$

restricting the problem to the situation in which $\mathbf{G}(A, \delta t, P)$ is a linear function of the free parameters:

$$\begin{aligned} \chi^2 = {} & (\mathbf{S} - A\mathbf{F} - (A\delta t)\mathbf{F}' - P\mathbf{1})^{\mathrm{T}} \mathbf{C}^{-1} \\ & \times (\mathbf{S} - A\mathbf{F} - (A\delta t)\mathbf{F}' - P\mathbf{1}) , \end{aligned} \qquad \text{(A.4)}$$

where $\mathbf{F}$ is a vector of $f(t_i)$, and $\mathbf{F}'$ is a vector of $\frac{\mathrm{d}f}{\mathrm{d}t}(t_i)$ and $\mathbf{1}$ has all its vector elements equal to 1. Minimizing χ^2 with respect to A, $A\delta t$ and P, a linear system of three equations is obtained:

$$\begin{pmatrix} \mathbf{F}^{\mathrm{T}}\mathbf{C}^{-1}\mathbf{F} & \mathbf{F}^{\mathrm{T}}\mathbf{C}^{-1}\mathbf{F}' & \mathbf{F}^{\mathrm{T}}\mathbf{C}^{-1}\mathbf{1} \\ \mathbf{F}'^{\mathrm{T}}\mathbf{C}^{-1}\mathbf{F} & \mathbf{F}'^{\mathrm{T}}\mathbf{C}^{-1}\mathbf{F}' & \mathbf{F}'^{\mathrm{T}}\mathbf{C}^{-1}\mathbf{1} \\ \mathbf{1}^{\mathrm{T}}\mathbf{C}^{-1}\mathbf{F} & \mathbf{1}^{\mathrm{T}}\mathbf{C}^{-1}\mathbf{F}' & \mathbf{1}^{\mathrm{T}}\mathbf{C}^{-1}\mathbf{1} \end{pmatrix} \begin{pmatrix} \hat{A} \\ \hat{A}\hat{\delta t} \\ \hat{P} \end{pmatrix} = \begin{pmatrix} \mathbf{F}^{\mathrm{T}} \\ \mathbf{F}'^{\mathrm{T}} \\ \mathbf{1}^{\mathrm{T}} \end{pmatrix} \mathbf{C}^{-1}\mathbf{S} . \qquad \text{(A.5)}$$

Denoting the matrix on the left of (A.5) as $\mathbf{M}$, the solution of the system can be expressed as

$$\begin{pmatrix} \hat{A} \\ \hat{A}\hat{\delta t} \\ \hat{P} \end{pmatrix} = \mathbf{M}^{-1} \begin{pmatrix} \mathbf{F}^{\mathrm{T}} \\ \mathbf{F}'^{\mathrm{T}} \\ \mathbf{1}^{\mathrm{T}} \end{pmatrix} \mathbf{C}^{-1}\mathbf{S} = \mathbf{W}\mathbf{S} , \qquad \text{(A.6)}$$

where $\mathbf{W}$ is the matrix of weights.

The covariance matrix $\mathbf{V}$ between the estimators is equal to

$$\begin{aligned} \mathbf{V} & = E[(\mathbf{WS} - E[\mathbf{WS}])(\mathbf{WS} - E[\mathbf{WS}])^{\mathrm{T}}] \\ & = \mathbf{W}\mathbf{C}\mathbf{W}^{\mathrm{T}} = \mathbf{M}^{-1} . \end{aligned} \qquad \text{(A.7)}$$

Replacing the parameters by the solutions of (A.6) in (A.4), the minimal χ^2 value can be computed:

$$\begin{aligned} \chi^2_{\mathrm{Min}} & = \mathbf{S}^{\mathrm{T}} (\mathbb{1} - (\mathbf{F}\mathbf{F}'\mathbf{1})\,\mathbf{W})^{\mathrm{T}} \mathbf{C}^{-1} (\mathbb{1} - (\mathbf{F}\mathbf{F}'\mathbf{1})\,\mathbf{W})\mathbf{S} \\ & = \mathbf{S}^{\mathrm{T}} \mathbf{M}_{\chi^2} \mathbf{S} , \end{aligned} \qquad \text{(A.8)}$$

where $\mathbf{M}_{\chi^2}$ is a matrix which can be used to compute χ^2_{Min} event-by-event without minimizing χ^2.

All simpler cases can be derived from (A.5) and (A.6). Two common cases are as follows.

1. The parameter A is the only free parameter. Simplifying (A.5) gives

   $$\mathbf{W} = \frac{\mathbf{F}^{\mathrm{T}}\mathbf{C}^{-1}}{\mathbf{F}^{\mathrm{T}}\mathbf{C}^{-1}\mathbf{F}} . \qquad \text{(A.9)}$$

   In addition, if $\mathbf{C} = \sigma^2 \mathbb{1}$:

   $$W_i = \frac{f_i}{\sum_j^N f_j^2} . \qquad \text{(A.10)}$$

   The variance of $\hat{A}$ is obtained from (A.7): $V(\hat{A}) = \frac{1}{\mathbf{F}^{\mathrm{T}}\mathbf{C}^{-1}\mathbf{F}} = \frac{\sigma^2}{\sum_j^N f_j^2}$.
2. The parameters A and P are free parameters and $\mathbf{C} = \sigma^2 \mathbb{1}$. Solving(A.5) gives two sets of weights used to compute the two estimators

$$\begin{pmatrix} \hat{A} \\ \hat{P} \end{pmatrix} = \frac{1}{N\mathbf{F}^{\mathrm{T}}\mathbf{F} - (\mathbf{F}^{\mathrm{T}}\mathbf{1})^2} \begin{pmatrix} N\mathbf{F}^{\mathrm{T}} - (\mathbf{F}^{\mathrm{T}}\mathbf{1})\mathbf{1}^{\mathrm{T}} \\ (\mathbf{F}^{\mathrm{T}}\mathbf{F})\mathbf{1}^{\mathrm{T}} - (\mathbf{F}^{\mathrm{T}}\mathbf{1})\mathbf{F}^{\mathrm{T}} \end{pmatrix} \mathbf{S} = \mathbf{W}\mathbf{S}\,. \tag{A.11}$$

The weights can also be written as

$$\begin{aligned} W_{A,i} &= \frac{f_i - \sum_j^N f_j}{\sum_j^N f_j^2 - \left(\sum_j^N f_j\right)^2 / N}, \\ W_{P,i} &= \frac{\sum_j^N f_j^2 - \left(\sum_j^N f_j\right) f_i}{N \sum_j^N f_j^2 - \left(\sum_j^N f_j\right)^2}\,. \end{aligned} \tag{A.12}$$

Equation (A.7) gives $V(\hat{A}) = \frac{\sigma^2}{\sum_j^N f_j^2 - (\sum_j^N f_j)^2/N}$.

3. Jitter-compensating weights can be obtained by leaving δt as a free parameter. In the case where A and δt are the only two free parameters and $\mathbf{C} = \sigma^2 \mathbb{1}$, the weights are computed as

$$\begin{aligned} \begin{pmatrix} \hat{A} \\ \hat{A}\hat{\delta t} \end{pmatrix} &= \frac{1}{(\mathbf{F}'^{\mathrm{T}}\mathbf{F}')(\mathbf{F}^{\mathrm{T}}\mathbf{F}) - (\mathbf{F}^{\mathrm{T}}\mathbf{F}')^2} \\ &\times \begin{pmatrix} (\mathbf{F}'^{\mathrm{T}}\mathbf{F}')\mathbf{F}^{\mathrm{T}} - (\mathbf{F}^{\mathrm{T}}\mathbf{F}')\mathbf{F}'^{\mathrm{T}} \\ (\mathbf{F}^{\mathrm{T}}\mathbf{F})\mathbf{F}'^{\mathrm{T}} - (\mathbf{F}^{\mathrm{T}}\mathbf{F}')\mathbf{F}^{\mathrm{T}} \end{pmatrix} \mathbf{S} = \mathbf{W}\mathbf{S}\,, \end{aligned} \tag{A.13}$$

which gives

$$W_{A,i} = \frac{\left(\sum_j^N \frac{\mathrm{d}f_j}{\mathrm{d}t}^2\right) f_i - \left(\sum_j^N f_j \frac{\mathrm{d}f_j}{\mathrm{d}t}\right) \frac{\mathrm{d}f_i}{\mathrm{d}t}}{\left(\sum_j^N f_j^2\right) \left(\sum_j^N \frac{\mathrm{d}f_j}{\mathrm{d}t}^2\right) - \left(\sum_j^N f_j \frac{\mathrm{d}f_j}{\mathrm{d}t}\right)^2}\,. \tag{A.14}$$

References

1. CMS Collaboration, The Compact Muon Solenoid Technical Proposal, CERN/LHCC 94-38, 1994
2. CMS Collaboration, The Electromagnetic Calorimeter Technical Design Report, CERN/LHCC 1997-033, 1997
3. V.G. Baryshevsky et al., Nucl. Instrum. Methods A **322**, 231 (1992)
4. Z. Antunovic et al., Nucl. Instrum. Methods A **537**, 379 (2005)
5. M. Apollonio et al., Nucl. Instrum. Methods A **532**, 566 (2004)
6. M. Raymond et al., The MGPA Electromagnetic Calorimeter Readout Chip for CMS, Proceedings of the 9th Workshop on Electronics for the LHC Experiments, CERN-LHCC-2003-055, 2003
7. P. Adzic et al., Eur. Phys. J. C **44**, 1 (2006)
8. P. Paganini, I. van Vulpen, Pulse amplitude reconstruction in the CMS ECAL using the weights method, CMS Note 2004/025
9. W.E. Cleland, E.G. Stern, Nucl. Instrum. Methods A **338**, 467 (1994)